Grid study for Delayed Detached Eddy-Simulation's grid of a pre-stalled wing

Violaine Huck, François Morency, Heloise Beaugendre

Grid study for Delayed Detached Eddy-Simulation's grid of a pre-stalled wing

Violaine Huck
Thermofluide pour le Transport, Ecole de Technologie Supérieure, Canada
violaine.huck@estaca.eu

François Morency
Thermofluide pour le Transport, Ecole de Technologie Supérieure, Canada
francois.morency@etsmtl.net

Héloïse Beaugendre
Bordeaux INP, INRIA Bordeaux, France
heloise.beaugendre@math.u-bordeaux.fr

Abstract:

For wing in medium or deep stalled configuration, strong vortices occur whereas the boundary layer still affects the aerodynamic coefficients' results. In the past recent years, RANS' model (Reynolds-Averaged Navier-Stokes) has been widely used to predict aerodynamic phenomena, but it showed its weakness in predicting the modulation in vortex shedding (Forsythe, Squires, Wurtzler, & Spalart, 2004; Liang & Xue, 2014). Concomitantly Large Eddy Simulation (LES) succeeds in modelling eddy phenomena, while it fails predicting boundary-layer's phenomena with the current computation's power (Mockett, 2009). Using the advantage of both methods, Delayed Detached Eddy-Simulation (DDES) shows better results, but the solutions given seem to show more sensitivity to grid refinement than RANS or LES (Forsythe et al., 2004). In order to spare time and resources while increasing the results' accuracy of the stalled wing configuration's aerodynamic coefficients, this study offers a parametric grid study for the DDES model. For three different grid refinements, characteristics of lift and eddy phenomena are presented and compared to determine, for an infinite wing, the best compromise between time and resources' consumption, and results' accuracy. Using the open software SU2 6.1 (Stanford University Unstructured), we generate three different types of grid refinements around an airfoil, developed spanwise to obtain a straight wing. On the same stalled configuration for each mesh, CFD solutions are ran with the DDES model, and the raw data are postprocessed with the open software ParaView 5.6. We then compare the aerodynamic coefficients' distributions obtained by the three mesh. The general modelling of vortex shedding's topology and turbulence viscosity are compared with the literature to ensure the right rendering of vortex structures. Chordwise pressure and friction coefficients' distributions as well as the spanwise lift coefficient are also compared. We conclude with the optimum mesh in term of results and resources' consumption.

Nomenclature :

M : Mach number
Vinf : upstream's velocity (m/s)
AOA : angle of attack
AR : Aspect Ratio
Re : Reynolds number
c : chord (m)
ρ: density
$\tilde{\nu}$: viscosity-like variable
Δy : spatial step of the mesh in the spanwise direction (m)
Δt : time-step (s)
Δt* : dimensionless time-step
RANS : Reynolds-Averaged Navier-Stokes

DES : Detached Eddy Simulation
DDES : Delayed Detached Eddy simulation

Introduction

Ice accretion on airfoils are highly critical for the aircraft envelop, for it changes the shape of the leading edge and more generally, the wing. Consequently, turbulent phenomenon occurs downstream of ice accretion, such as separation bubble, which highly affect the aerodynamics characteristics of the airplane and can even decrease the critical angle of attack, angle at which the aircraft stalls. Consequently, industrial growing of interest for the limit conditions of aircraft envelops drove current studies to investigate unsteady flow with high Reynolds number (Mockett, 2009, p. 48) (Deck, 2011). Indeed, when a stalled configuration occurs, the flow becomes strongly turbulent and strong eddies appear downstream the wings. To numerically predict this type of phenomenon, several numerical methodologies for Computational Fluid Dynamics (CFD) exist and each of them are accurate and resource consuming to a certain extend. The most accurate one is the Direct Numerical Simulation (DNS), which is also the most power consuming one. However, as current computers cannot withstand its expensive computation of complex geometries' simulation, several models have been created to reduce power consumption at the expense of accuracy. Each of these models are an outcome of specific Direct Numerical Simulation's simplifications for a particular problem (Mockett, 2009, p. 49) thus, it is of high importance to well understand the motivations behind each model. The most widely used, the Reynolds Averaged Navier-Stokes (RANS) has been widely spread among the aeronautical industries for the last 30 years. However, it showed its weakness in predicting the modulation in vortex shedding (Forsythe et al., 2004, p. 193; Liang & Xue, 2014)**.** Concomitantly, Large Eddy Simulation's (LES) governing equations are 3D and unsteady just as DNS, but with a close difference: small eddies are modelled, and bigger ones are resolved by the grid to reduce the expense compare to DNS. With the increase of computational resources, LES (Mockett, 2009, p. 40) is now used for application where influence of the wall is not crucial (Deck, 2011)**.** Nonetheless, its computational cost keeps its application for wall bounded flows with high Reynolds number out of reach for industrial (Mockett, 2009, p. 48).

LES suits well to predict strongly turbulent flows, but, with the current computer's power, lacks the accuracy for predicting the boundary layers' phenomenon, where RANS predictions are generally righteously. Stated by Spalart *et al.* in 1997, the Detached Eddy-Simulation (DES) ally the advantages of these two models. DES uses RANS model for the attached boundary layer and LES for the separated flow. The advantage of this model is its cost, less expensive than LES especially for high Reynolds number, and its accuracy compare to RANS, for unsteady and 3D flow. To date, predictions using DES had been conclusive (Forsythe et al., 2004). The definition of DES as stated in its original form by Spalart *et al.*, 1997, DES97 : "A Detached-Eddy Simulation is a three-dimensional unsteady numerical solution using a single turbulence model, which functions as a sub grid-scale model in regions where the grid density is fine enough for a large-eddy simulation, and as a Reynolds-averaged model in regions where it is not." . The phenomenon dictating the RANS/ LES transition is thus the detached or attached state of the local flow. The Delayed Detached Eddy-Simulation (DDES) is one of the first improvement of DES, which cope with the abnormal intrusion of LES mode in the boundary layer, the grid-Induced activation of the LES mode in boundary layer, and which induces an early detachment of the flow (Spalart et al., 2006). As DDES is a non-zonal method and defines the regions where RANS and LES are active, it constitutes then a good option for iced airfoils studies at high Reynolds number.

The literature has investigated the accuracy of DDES predictions for iced airfoils at several angles of attack, in comparison with other mathematical models, such as RANS (Alam, Thompson, & Walters,

2015), Improved Detached Delayed Eddy Simulation (IDDES) (Hu, Zhang, Liu, Wang, & Li, 2018), or DES (Lorenzo, Valero, & de-Pablo, 2011). Zhang, Habashi, and Khurram (2016) and Oztekin and Riley (2018) have explored, for Zonal Detached Eddy Simulation and DDES, the influence of both the span domain size and the grid density on simultaneously two spatial dimensions but the spanwise. These studies came all up with spanwise spatial steps Δy/c that can vary by three order of magnitude depending on the study (Pan & Loth, 2004) (Butler, Qin, & Loth, 2016). Nevertheless, none of them has specifically studied the influence of the Δy/c parameter alone on the aerodynamic coefficients' accuracy of an iced airfoil at a near stalled angle. This parameter is critical to capture eddies downstream of ice horns. Xiao, Zhang, and Chen (2017) have enlighten the influence of grid density on aerodynamic coefficient. Their study shows that though lift coefficient value gets closer to experimental data with mesh refinement, the drag coefficient accuracy doesn't go by this rule and is more ambiguous to improve. This present study aims to underpin the State of the Art on the DDES solution's behaviour depending on Δy/c parameter, for an iced airfoil in a near stalled configuration.

The table 1 briefly presents solutions' characteristics for straight iced wings, at high Reynolds number and low Mach number, in the state of the art, using DES, DDES, ZDES and IDDES. These mathematical methods are all improvements of the original Detached Eddy Simulation model, DES97. The type of model is identified on the first columns on the left, while each line summarizes the flow field parameters, the span wise grid spacing, and the time step used for the calculations. Dimensionless time-steps are calculated as follow: $\Delta t^* = \frac{\Delta t V_{inf}}{c}$. As can been seen, time step and span wise grid spacing vary greatly from one study to another, with no clear correlation to neither the Reynolds number nor the Mach number.

Table 1: State of the art

model	**year**	**author**	**M**	**Vinf**	**Re**	**Δy/c**	Δt	Δt*
DDES	**2015**	M. F. Alam, David S. Thompson and D. Keith Walters	0,12		3,50E+06		5,00E-06	2,25E-04
DDES	**2018**	Ezgi S. Oztekin, James T. Riley	0,18		1,80E+06	3,00E-03		5,00E-04
DES	**2004**	Jianping Pan, Eric Loth	0,21		2,00E+06	1,00E-02		1,00E-03
DES	**2004**	Jianping Pan, Eric Loth	0,185		1,80E+06	1,00E-02		1,00E-03
ZDES	**2016**	(Zhang, Habashi, & Khurram, 2016)	0,12	39,381	1,66E+05		1,00E-05	1,00E-03
			0,2	65,635	1,59E+07		1,00E-05	1,00E-03
DDES	**2017**	Maochao Xiao, Yufei Zhang and Haixin Chen	0,21	39,381	6,00E+06	2,00E-03	3,00E-05	1,30E-03
DES	**2004**	Jianping Pan, Eric Loth	0,3		3,00E+06	4,76E-02		1,00E-02
IDDES & DDES	**2016**	Cameron Butler, Chao Qin, Eric Loth	0,171	58,15584	1,80E+06	1,33E-05	1,00E-03	1,27E-01
DDES	**2011**	Lorenzo A., Valero E., de-Pablo V.	0,2		3,00E+6	2,899E-3	6,25e-6	
						1,99 E-3		
						1,995 E-3		

In the table 1: (DES: Detached Eddy Simulation ; ZDES : Zonal Detached Eddy Simulation ; IDDES : Improved Delayed Detached Eddy Simulation).

Using an industrial 2D hybrid O-mesh of a Model 5-6 iced airfoil homogeneously spanwise expanded, the main issue of this study is to determine the optimum Δy to obtain satisfying results with DDES, based on aerodynamic coefficients accuracy to the experimental data and Q-criterion for the vortex structures. The Model 5-6 profile is in a pre-stall configuration, at an AOA=8° (Lorenzo et al., 2011), with a chord unity, a Mach number of 0.2 and Reynolds number of 3,0 million.

Three different meshes are built with three different span-step Δy, from coarse to fine. DDES simulations are run with the conditions mentioned above. Results are compared for validation and verification with literature (GARTEUR, 2003; Lorenzo et al., 2011; Tagawa, Morency, & Beaugendre, 2018). The different meshes are compared regarding four aspects: general aspect of vorticities iso-contours, Q-criterion iso-contours, aerodynamics coefficients' value and distributions and streamlines' reattachment localisation.

In this paper, we will first introduce the numerical model, section II, and the numerical methods based on the state of the art, section III. Then, in section IV, validation cases are presented for DDES simulations, using data extracted from GARTEUR (2003). Finally, section V discusses the spanwise grid density's influence on aerodynamic coefficients.

II- Mathematical Model

The DDES model implementation of the open software Stanford University Unstructured (SU2), version 6.0.1, is used, with the Spalart-Allmaras (SA) turbulence model (Molina & Silva, 2017). Simulations are first ran using RANS model and SA turbulence model until convergence. The results of the simulation ar then used to initialize DDES model calculation.

The 3D flows are modeled by the compressible, turbulent Navier-Stokes equations, expressed in the conservative form (Molina et al., 2017). The vector of conservative variables is

$$U = (\rho, \rho v_1, \rho v_2, \rho v_3, \rho E)^T \tag{1}$$

where ρ is the air density, E is the total energy per unit mass, and $\vec{v} = (v_1, v_2, v_3) \in \mathbb{R}^3$ is the flow velocity in Cartesian coordinate system. Then, the Navier-Stokes equations are expressed as a general convection diffusion equation

$$\frac{\partial U}{\partial t} + \nabla \cdot \overrightarrow{F^c} - \nabla . \vec{F}^v - Q = 0 \tag{2}$$

on a domain $\Omega \subset \mathbb{R}^3$, $t > 0$, with the convective fluxes defined as

$$\overrightarrow{F_i^c} = \begin{pmatrix} \rho v_i \\ \rho v_i v_1 + P\delta_{i1} \\ \rho v_i v_2 + P\delta_{i2} \\ \rho v_i v_3 + P\delta_{i3} \\ \rho v_i H \end{pmatrix}, \tag{3}$$

and the viscous fluxes defined as

$$\overrightarrow{F_i^v} = \begin{pmatrix} \dot{\tau}_{i1} \\ \tau_{i2} \\ \tau_{i3} \\ v_j\tau_{ij} + \mu^*_{tot}C_p\partial_i T \end{pmatrix} \quad (4)$$

For $i = 1,2,3$. The source term Q is 0 for the aerodynamic problems studied here. P is the static pressure, H is the fluid enthalpy, T is the temperature, and δ_{ij} is the Kronecker delta function.

Assuming that the perfect gas law holds, with a constant ratio of specific heat, γ, and gas constant R, the pressure is determined from

$$P = (\gamma - 1)\rho[E - 0.5(\vec{v}.\vec{v})] \quad (5)$$

$C_P = \gamma R/(\gamma - 1)$ is the specific heat of air at constant pressure, and the temperature is defined as

$$T = \frac{P}{\rho R} \quad (6)$$

In this paper, unsteady turbulent flows are solved with suitable turbulent models based on the Boussinesq hypothesis (White, 2006) and the viscous stresses are written as:

$$\tau_{ij} = \mu_{tot}(\partial_j v_i + \partial_i v_j - \frac{2}{3}\delta_{ij}\nabla.\vec{v}) \quad (7)$$

and

$$\mu_{tot} = \mu_d + \mu_t \text{ and } \mu^*_{tot} = \frac{\mu_d}{\mathrm{Pr}_d} + \frac{\mu_t}{\mathrm{Pr}_t} \quad (8)$$

The dynamic viscosity μ_d is assumed to satisfy Sutherland's law (White, 2006). The turbulent viscosity μ_t is obtained from the one equation turbulent model of Spalart-Allmaras (SA) model (P. Spalart & Allmaras, 1992). The original model is modified such that a modified wall distance is used, enabling RANS modeling near the walls and LES modeling elsewhere (P. Spalart, 2000).

A. Spalart-Allmaras (SA) model

The hybrid RANS/LES model used in this paper is based on the original SA model (P. Spalart & Allmaras, 1994). The turbulent viscosity is computed from

$$\mu_t = \rho\hat{\nu}f_{v1},\ f_{v1} = \frac{\chi^3}{\chi^3 + c^3_{v1}},\ \chi = \frac{\hat{\nu}}{\nu},\ \nu = \frac{\mu_d}{\rho} \quad (9)$$

The transport equation for the new variable $\hat{\nu}$ is

$$\frac{\partial\hat{\nu}}{\partial t} + v_j\frac{\partial\hat{\nu}}{\partial x_j} = c_{b1}(1 - f_{v2})\hat{S}\hat{\nu} - \left[c_{\omega 1}f_\omega - \frac{c_{b1}}{\kappa^2}f_{v2}\right]\left(\frac{\hat{\nu}}{d}\right)^2 + \frac{1}{\sigma}\left[\frac{\partial}{\partial x_j}\left((\nu + \hat{\nu})\frac{\partial\hat{\nu}}{\partial x_j}\right) + c_{b2}\frac{\partial\hat{\nu}}{\partial x_i}\frac{\partial\hat{\nu}}{\partial x_i}\right] \quad (10)$$

where the production term is based on the fluid vorticity $\vec{\omega}$ and d, the distance from the nearest wall

$$\hat{S} = |\vec{\omega}| + \frac{\hat{\nu}}{\kappa^2 d^2} f_{\upsilon 2},\ \vec{\omega} = \nabla \times \vec{\upsilon} \tag{11}$$

and

$$f_{\upsilon 2} = 1 - \frac{\chi}{1 + \chi f_{\upsilon 1}},\ f_{\omega} = g\left[\frac{1 + c_{\omega 3}^6}{g^6 + c_{\omega 3}^6}\right]^{1/6},\ \text{where}\quad g = r + c_{\omega 2}\left(r^6 - r\right) \text{and}\ r = \frac{\hat{\nu}}{\hat{S}\kappa^2 d^2} \tag{12}$$

The closure constants are:

$$\sigma = 2/3,\ c_{b1} = 0.1355,\ c_{b2} = 0.622,\ \kappa = 0.41,\ c_{\omega 1} = \frac{c_{b1}}{\kappa^2} + \frac{1 + c_{b2}}{\sigma},\ c_{\omega 2} = 0.3,\ c_{\omega 3} = 2,\ c_{\upsilon 1} = 7.1 \tag{9}$$

In the context of the general convection diffusion equation

$$\vec{F}^{c} = \vec{\upsilon}\hat{\nu},\ \vec{F}^{\upsilon} = \frac{\nu + \hat{\nu}}{\sigma}\Delta\hat{\nu},\ \mathrm{Q} = c_{b1}(1 - f_{\upsilon 2})\hat{S}\hat{\nu} + c_{b2}\frac{\partial\hat{\nu}}{\partial x_i}\frac{\partial\hat{\nu}}{\partial x_i} - \left[c_{\omega 1} f_{\omega} - \frac{c_{b1}}{\kappa^2} f_{\upsilon 2}\right]\left(\frac{\hat{\nu}}{d}\right)^2 \tag{13}$$

The boundary conditions are

$$\hat{\nu}_{wall} = 0 \text{ and } \hat{\nu}_{farfield} = 3\nu \tag{14}$$

B. Delayed Detached Eddy Simulation

The Detached Eddy Simulation (DES) proposed to switch from RANS to LES model is based on a modified length scale definition $\overline{d}$, used instead of the distance from the nearest wall, d, in the SA model (PR Spalart, Jou, Strelets, & Allmaras, 1997) . The length scale is based on the local maximum grid spacing Δ :

$$\overline{d} = \min(d, C_{DES}\Delta) \tag{15}$$

$$\Delta = \max(\Delta_x, \Delta_y, \Delta_z) \tag{16}$$

The value of C_{DES} =0.65 is obtained after calibration on isotropic turbulence. Usually, the maximum grid spacing should be larger than the boundary layer because the elements near the wall are highly stretched in the streamwise direction for most aerodynamic flows. However, in some particular cases, the maximum grid spacing could be smaller than the boundary layer and lead to activation of LES inside the attached boundary layer region. To prevent this situation, the Delayed Detached Eddy Simulation (DDES) model has proposed a new length scale definition (P. R. Spalart et al., 2006):

$$\tilde{d} = d - f_d \max(0, d - C_{DES}\Delta) \tag{17}$$

$$f_d = 1 - \tanh((8r_d)^3),\ r_d = \frac{\nu + \hat{\nu}}{\sqrt{U_{i,j}U_{i,j}\kappa^2 d^2}} \tag{18}$$

Where $U_{i,j}$ is the velocity gradient, κ is the Karman constant. The function f_d is zero in RANS region. Although a powerful tool, the DDES still have some issues, with free shear layers for example. The main challenge is to correctly identify the RANS and LES area, especially in the case of unstructured grid and anisotropic grid cell typically used in industrial problems.

C. Shear-Layer Adapted DDES

The Shear-layer Adapted model proposed a new length scale definition that tries to correct the anisotropic grid cell effects on the RANS/LES transition (Shur, Spalart, Strelets, & Travin, 2015). The length scale takes into account the direction of the vorticity vector. For a cell with the center vector $\vec{r}$ and vertices located at $\vec{r_n}$ and being the number of element vertices (8 for hexahedral cell), the definition is

$$\tilde{\Delta}_\omega = \frac{1}{\sqrt{3}} \max_{n,m=1,8} \left| \vec{I}_n - \vec{I}_m \right|, \ \vec{I}_n = \vec{n}_w \times \vec{r}_n \tag{19}$$

where $\vec{n}_w$ is the unit vector aligned with the vorticity vector. The length scale is further corrected to facilitate the Kelvin Helmhotz instability in the case the grid is marginal in its ability to resolve the Kelvin Helmhotz instability, thus

$$\Delta = \Delta_{SLA} = \tilde{\Delta}_\omega F_{KH} \left(\langle VTM \rangle \right) \tag{20}$$

The F_{KH} function depends on the average values VTM (Vortex Tilting Measure) over the current and closest neighboring cells, $\langle VTM \rangle$. The piecewise linear function is defined as

$$F_{KH} \left(\langle VTM \rangle \right) = \max \left(F_{KH}^{\max}, F_{KH}^{\min} + \frac{F_{KH}^{\max} - F_{KH}^{\min}}{a_2 - a_1} \left(\langle VTM \rangle - a_1 \right) \right) \tag{21}$$

Here $F_{KH}^{\max} = 1.0$, $F_{KH}^{\min} = 0.1$, $a_1 = 0.15$, and $a_2 = 0.3$. Finally, the definition of VTM is

$$VTM = \frac{\sqrt{6} \left| \left(\hat{S} \cdot \vec{\omega} \right) \times \vec{\omega} \right|}{\omega^2 \sqrt{3tr(\hat{S}^2) - \left[tr(\hat{S}) \right]^2}} \max(1, \nu^* / \nu_t), \ \nu^* = 0.2\nu \tag{22}$$

The COARSE, the MEDIUM and the FINE meshes, are created from the same 2D hybrid O-mesh of an iced Model 5-6 airfoil, which is expanded on the span direction to create a 3D mesh. The span domain is 1c for the COARSE and the MEDIUM mesh, and 0.402c for the FINE mesh for resources sparing. The number of layers in the span direction is the only parameter that changes from one mesh to another, and we refer to it in this paper as Δy, as the spatial step in the y direction. The boundary conditions are set periodic, to allow flow in the y direction for turbulences modelling purposes. The scheme of the problem is presented on Figure 1. At the forefront, a zoom on the 5-6 Model iced airfoil meshed. The initial conditions are exposed, with the Mach number at 0.2 the angle attack at 8° and the Reynolds number at 3.0E6. Aft of the zoom, we see the 2D hybrid O-mesh. The 2D O-mesh is then expended in the span (y) direction, until the plan Y=1. The main issue discussed in this study is the value of the spanwise step Δy.

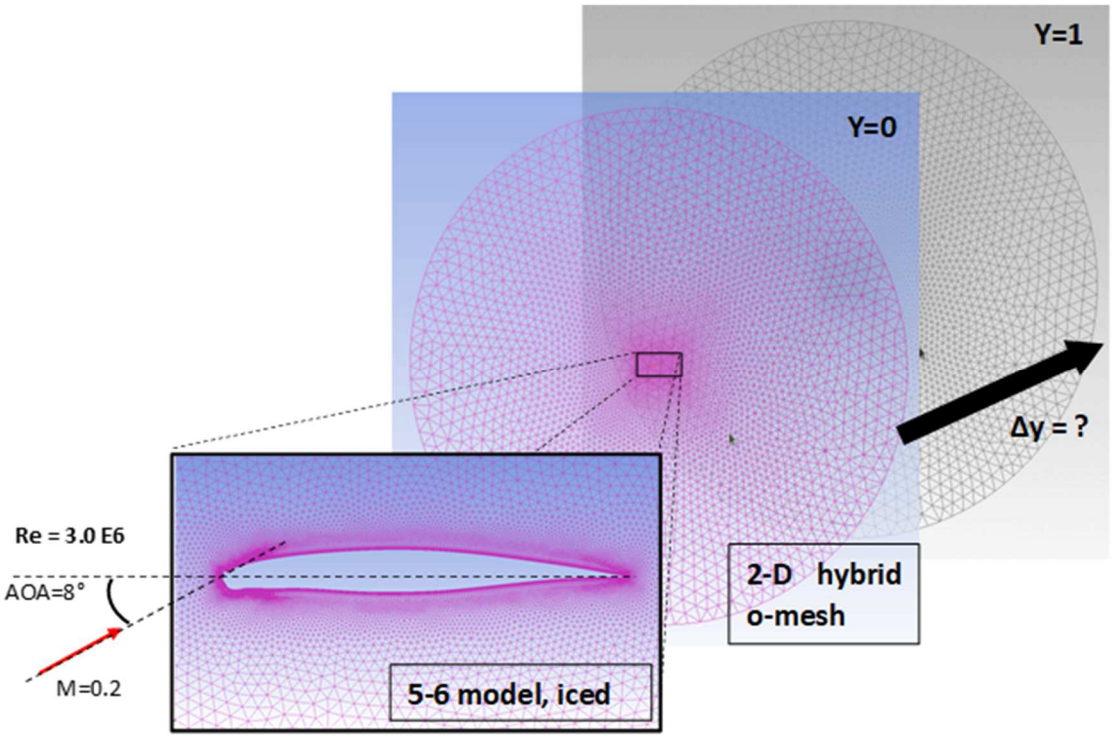

Figure 1: Scheme of the problem

The free stream initial conditions for the three meshes are presented in Table 2. Aerodynamic coefficients are plotted around the Model 5-6 iced wing and free stream is at an angle of attack of 8°. We select a low Mach number M=0,2, a high Reynolds number Re=3,0E6. Conditions on the wall are set adiabatic. Table 3 sum up the specific constants used for the Delayed Detached Eddy Simulations. According to literature, we chose a time-step of Δt=5E-6s such as the CFL number is approximatively unity downstream of the horn. The boundary conditions are set periodic. The viscosity and the turbulence model are respectively Sutherland model and Spalart-Allmaras model for the RANS region. We use a Roe low dissipation and Flow convective numerical method as recommended in Molina et al (2017). The time discretization is 2nd order Euler implicit and the numerical method for spatial gradients is the weighted least square method.

Table 2: Free stream definition

test case	domain	M	Re	AOA	fluid	Temperature
Iced wing, Model 5-6	3D	0.2	3.0E6	8°	viscous	288.15 K

Table 3: Specific constants and model for DDES simulations

Δt	Δt*	Cdes	Boundary Conditions	Viscosity model	Turbulence model
5E-6	1.70E-4	0.65	Periodic ; adiabatic wall	Sutherland	SA/EDDES
Roe Low dissipation ((Molina & Silva, 2017)	Flow Convective numerical method	Slope Limiter flow	Time discretization	Numerical method for spatial gradients	
NTS	SLAU2	Venkatakrishnan	2nd order Euler implicit	Weighted least square	

III- Numerical Method

According to the literature, see table 1, we set three different non dimensional spatial spanwise steps from 4E-2 to 6E-3. The table 4 presents the different characteristics of the three meshes, i.e. total elements, total nodes, spatial spanwise step Δy/c made dimensionless with the chord length. The COARSE and the MEDIUM meshes have been set with a span domain's size equal to the chord length. This specific configuration have been referred as appropriate for a pre-stalled configuration (Zhang et al., 2016), which is the chosen configuration in this present study.

However, aware of the importance of critical computational resources, and for the sake of sparing time and resources, the fine mesh has been set with a smaller span domain's size. Literature (Pan & Loth, 2005) recommend a domain size of at least twice the size of the separation bubble's height obtained in a RANS simulation for the configuration of interest. According to the RANS results we obtained with the periodic boundary conditions and the SA turbulent model, the separation bubble's height does not exceed 0.1c. However, Zhang et al. (2016) found that this constant value was not satisfactory when approaching the stalled configuration, and concluded for their iced airfoil, that a spanwise domain's size of 0.3c was satisfactory. Lorenzo et al. (2011), using the same iced airfoil in the same freestream conditions as we do in this present study, found that a span domain of 0.4c was an optimum setup for the iced Model 5-6 at AOA=8°. Given the conclusion of Zhang et al. (2016), given the conclusion of Lorenzo et al. (2011) regarding the poor influence of a greater span domain's size on the CL and CD values, given that we intend to study these coefficients, the fine mesh has been set with a span domain's size of 0.402c.

Table 4: Mesh's characteristics

Mesh	Total elements	Total nodes	chord	Δy/c	X/c	Y/c	Z/c
Coarse	1 596 198	1 129 674	1m	0,04	-22,0836 22,3017	-1 0	-22,2066 22,1787
MEDIUM	6 035 422	4 388 349	1m	0,01	-22,0836 22,3017	-1 0	-22,2066 22,1787
Fine	4 082 094	2 954 532	1m	0,006	-22,0836 22,3017	-0.402 0	-22,2066 22,1787

IV- Verification and Validation

First, the RANS simulations are run for each test case until convergence of the residuals and stabilisation of CL and CD values (around 40 000 iterations), to initialise the solution before running DDES.

In DDES, after some iterations, we start averaging the lift and drag coefficients at each time-steps. Table 5 sum-up for each mesh the range used for averaging. These ranges are selected according to the behaviour of both CL and CD through time. However, as literature does not bring to the fore a method for picking start and end of averaging, comparing mean values may lead to artificially increase or decrease relative errors, depending on the criterion favoured by each party.

Table 5: Sum up of the averaging range for each case

CASE	COARSE	THE MEDIUM	FINE
RANGE (iterations)	50 000 ; 70 000	50 500 ; 60 000	35 000 ; 50 000

As this present study mainly focus on lift and drag coefficients' prediction, both verification and validation case will lean on the mean aerodynamic coefficients' values.

A-Verification

Considering the same averages discussed above, we compare the mean CL and CD with values from literature. The data from the Lorenzo et al. (2011) against which our results are compared in table 6 (Ref DDES), have been obtained using DDES model on the same Model 5-6 iced wing model. DDES model used in Lorenzo et al (2011) is however not the same as the shear layer adapted DDES was not available at that time.

According to the relative errors from table 6, the COARSE mesh seems too coarse and fails to predict drag coefficient, with relative error of -55.9% compared to reference. Prediction of lift coefficient seems surprisingly good, with less than 5% of error. Four times finer than the COARSE mesh, the MEDIUM mesh shows really good results with relative errors for both mean CL and CD below 4%. The MEDIUM mesh already has, compared to literature, 1.03% of relative error for mean CL and with 3.26% of relative error, for mean CD, even though the MEDIUM mesh is five times coarser than literature's mesh. However, this similarity in the results can be caused by the difference in the DDES model used, knowing that literature's DDES model is not implemented with the shear layer adapted model, not available at the time.

Finally, it is the FINE mesh that shows the closest mean lift and drag coefficients to the one from literature, with a relative error of 0.0650% for mean CL and -2.67% for mean CD.

Table 6: Mean CD and CL comparison between results from the COARSE, THE MEDIUM, FINE meshes and results from Lorenzo et al. (2011) for iced Model 5-6 at AOA = 8°

case	CL	CD	%CL relative error against reference	%CD relative error against reference	Δy/c
Ref DDES	0.948	0.0834			0,002
COARSE	0.905	0.130	4.54	-55.9	0,04
MEDIUM	0.938	0.0861	1.03	-3.26	0,01
FINE	0.947	0.0857	0.0650	-2.67	0,006

B- Validation case

The experimental data are from the institute GARTEUR (2003). Experiments are carried out on a Model 5-6 iced with a chord length of 0,6759m and a span of 2,25m, referenced there as Model C1. The Mach number is 0.2 and the Reynolds number 3.0E6. The ice accretion shape, referred as IS1, is the same as the one depicted on this present study. Table 7 compares lift and drag coefficients against experimental data (GARTEUR, 2003). The last two columns display relative errors between simulations and experiences. To keep in mind the relative error found in Lorenzo et al, their results are displayed in the line "Ref DDES".

For the three cases, the mean CL relative errors are under 4% of error, with improvements of results with the mesh refinement. The gap of relative errors against experimental data between the COARSE and the MEDIUM mesh, which is four times finer, shows how sensitive DDES results are to grid refinement. The mean CL is already of good quality (under 1% relative error) with the MEDIUM mesh, whereas the mean CD remains acceptable with below 5% relative error, against 0.773% for numerical results from literature. In contrast, the COARSE mesh fails to predict CD, showing a relative error of

57.1%. Finally, the FINE mesh improved results for the mean CD, with a relative error of -3.46% compared to 4.07% for the MEDIUM mesh, but, at the same time, decrease the accuracy of the mean CL, with a relative error of -1.11% against -0.132% for the MEDIUM mesh. This relative error remains though acceptable, as around 1%.

Table 7: Mean CD and CL comparison from the different mesh, against experimental data GARTEUR (2003) for iced Model 5-6 at AOA = 8°

case	CL	CD	%CL relative error against experiment	%CD relative error against experiment	Δy/c
experimental	0.932	0.08276			
COARSE	0.905	0.130	3.42	-57.1	0.04
MEDIUM	0.938	0.0861	-0.132	-4.07	0.01
FINE	0.947	0.0856	-1.11	-3.46	0.006
Ref DDES	0.948	0.0834	-1.173959	-0.77332	0.002

The MEDIUM and fine meshes have been both validated and verified. The COARSE mesh is found to be too coarse. The relative error for the mean drag coefficient is found to be better for FINE mesh, with an improvement of 0,6% of the mean CD's relative error, whereas the mean lift coefficient is found to be better for the MEDIUM mesh, with 0,976% of difference between both CL's relative errors. Improvement of the relative error between the COARSE and the MEDIUM mesh is huge, with 53% difference. Considering the FINE mesh is 1,6 times finer than the MEDIUM mesh, this improvement is not as great as the one between the COARSE and the MEDIUM.

C- Mean Cp distribution

The mean pressure coefficient distributions are also compared against literature and experimental data. Figure 2 represents Cp distribution of experimental data (red plus), data from literature (black cross), and mean Cp values for the COARSE (dot line), the MEDIUM (dash line) and the FINE (solid line) meshes. In their report, authors from GARTEUR state that "pressure distributions are available, although pressures at the glace ice shape location are not considered accurate". Knowing the ice shape extending until 3%c on suction side and 15%c on the pressure side, we will not focus on these regions.

The mean Cp distribution of the COARSE mesh shows that whereas the mean CL has been found close to the experimental data, the mean Cp chordwise distribution fails to match the experiments. Indeed on the suction side, COARSE mesh over predicts the pressure plateau both seen in the experimental data and the literature on the first 20% of the chord. The COARSE mesh's pressure plateau extends until 47% of the chord, where experimental data present a much shorter pressure plateau, on 15% of the chord. Its value is also under predicted by the COARSE mesh by 33%. The pressure side is however well predicted by the COARSE mesh. However, as the region of interest is mostly located downstream of the horn, i.e. where the detachment bubble is located, we conclude that the COARSE mesh is too coarse and highly unsuitable for DDES simulation to predict aerodynamic coefficients.

The MEDIUM mesh shows a much better agreement with both the literature and the experimental data. The pressure plateau value is over predicted with a relative error below 7%, as we found in literature. Three bumps are noticed at respectively 15%c, 25%c and 40%c that can have been caused by a too short average range. Indeed, these bumps seems to be pressure constant localisations, which can be caused by the formation of other local separation bubble. However, except for these three bumps, the MEDIUM mesh well predicts the Cp distribution for both suction and pressure side. The MEDIUM mesh also over predict the pressure plateau length, which extends until 25%c against 15%c for experimental data. The FINE mesh shows better agreement with the experimental data: the

pressure plateau is closer to the experimental points and the three bumps have disappeared. The pressure plateau length is still over-predicted and extends until 20%c against 15%c for the experimental data.

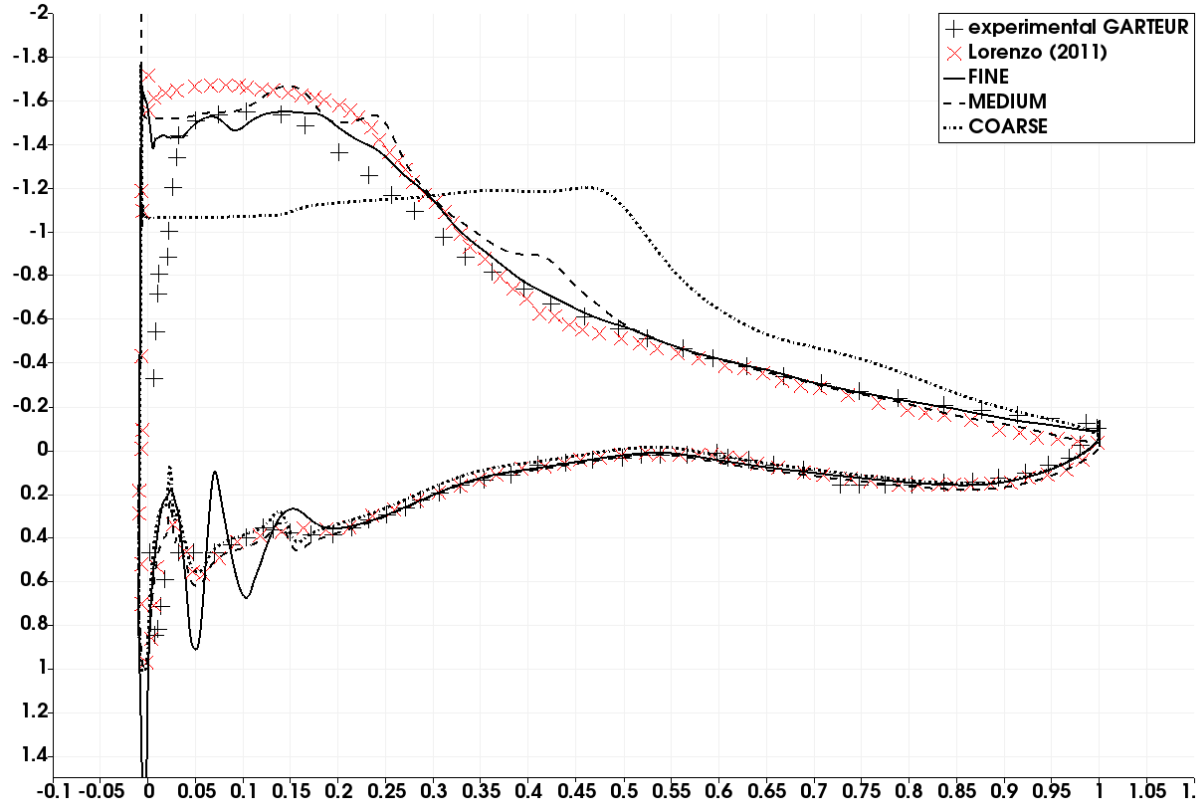

Figure 2: Mean Cp distributions comparisons of the COARSE, MEDIUM, FINE mesh against literature and experiment, for iced Model 5-6 at AOA = 8°, M=0.2, Re=3.0E6

Finally, it is the FINE mesh's mean Cp distribution that match better experiment's, with the closest pressure plateau length to experimental data. The MEDIUM mesh shows also a good mean CP distribution, with a close match with mean Cp distribution from literature.

VI-Spanwise grid density's influence

Identification of vortex structures can be done using different indicators, though some of them are more ambiguous than others, and if streamlines and pressure contours can help for identification of possible vortices, they are not sufficient to draw a conclusion on their existence, and neither is the vorticity magnitude (Bonnet, 1996). Bonnet (1996) defines what is expected for an effective vortex identification: nonzero circulation (vorticity) and Galilean invariant indicator. Two Galilean invariant indicators are usually used for coherent structure's identification : complex eigenvalues of the velocity gradient tensor, so called Δ criterion (Chong, Perry, & Cantwell, 1990) and second invariant of velocity gradient tensor, so called Q-criterion (Hunt, Wray, & Moin, 1988). This present study presents comparison of vortices structures using Q-criterion.

Figures 3 that follow present the instantaneous iso-surface of Q-criterion, Q=100000, for the COARSE, MEDIUM and the FINE meshes, respectively for the Figure 3.1, 3.2, 3.3. The Figure 3.4, from literature (Lorenzo, 2011), presents instantaneous iso surface of Q-criterion =1000000.

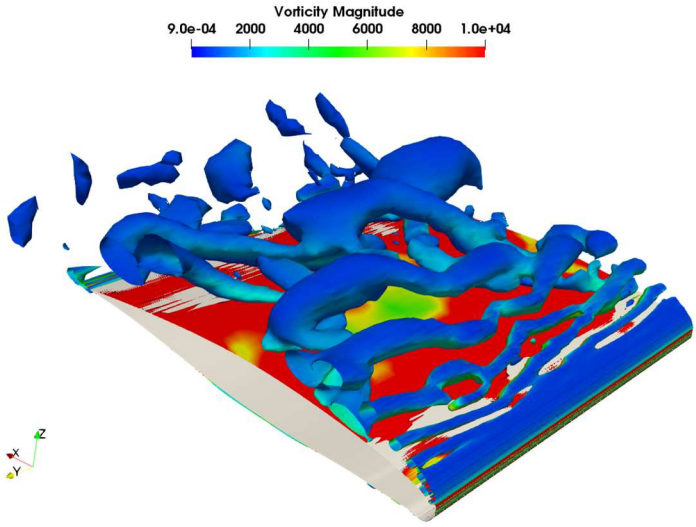

Figure 3.1: Instantaneous iso-surface iso-Q-criterion coloured by vorticities contours at 20200Δt, coarse mesh

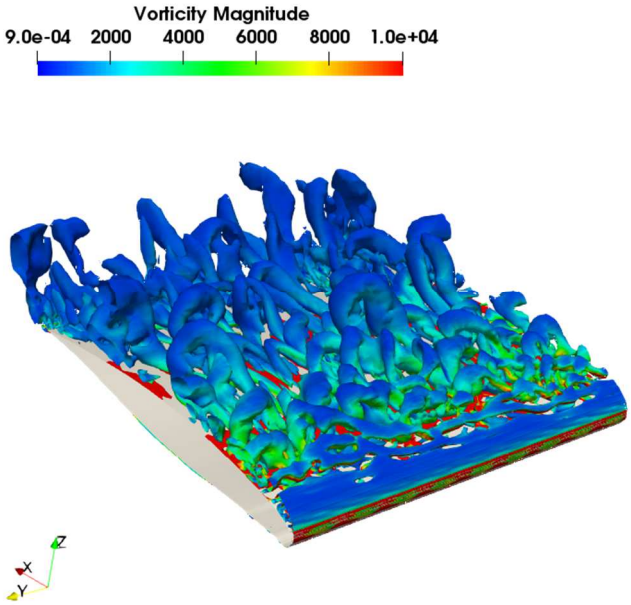

Figure 3.2: Instantaneous iso-surface iso-Q-criterion coloured by vorticities contours at 37200Δt, the MEDIUM mesh

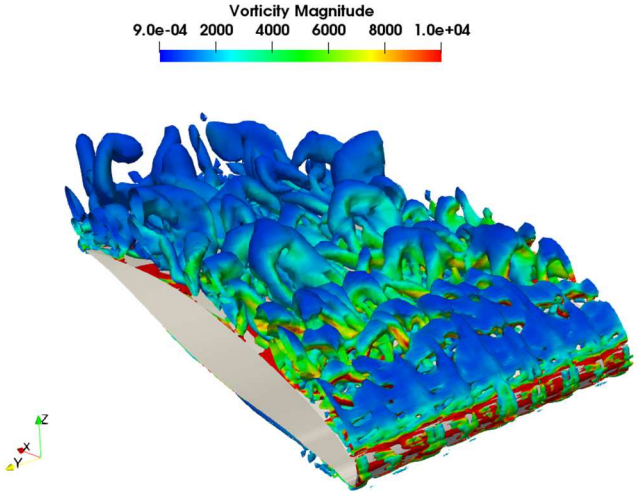

Figure 3.3 : Instantaneous iso-surface iso-Q-criterion coloured by vorticities contours at 24000 Δt, fine mesh

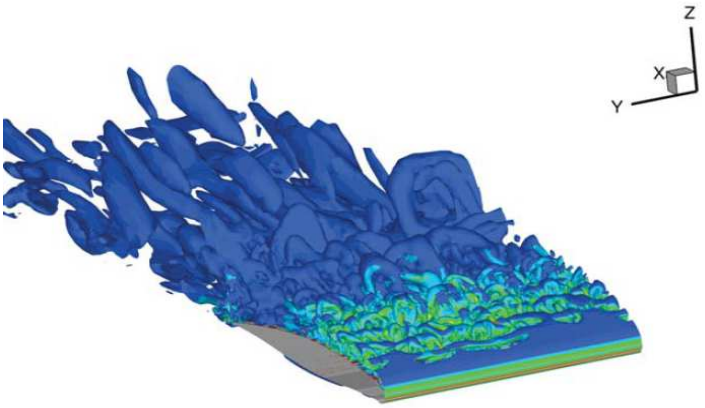

Figure 3.3: Iso-surfaces of Iso-Q = 1E6, coloured by vorticity (Lorenzo et al., 2011)

The velocity gradient tensor

$$\overline{\overline{\nabla}} u = \frac{\partial u_i}{\partial x_j}$$

$$\overline{\overline{\nabla}} u = \bar{\bar{S}} + \overline{\overline{\Omega}}$$

As a tensor can be decomposed as the sum of a symmetric tensor $\bar{\bar{S}}$ and skew-symmetric $\bar{\bar{\Omega}}$; where $\bar{\bar{S}}$ is the Strain of rate tensor, and $\bar{\bar{\Omega}}$ is the vorticity tensor.

The characteristics equation of the velocity gradient tensor can be written:

$$\lambda^3 - P\lambda^2 + Q\,\lambda - R = 0 \qquad (23)$$

Where P, Q and R are respectively the first, second and third invariant of the velocity gradient tensor (Bonnet, 1996). The Q-criterion, defined as Q>0, highlights places where the vorticity forces are at least (Q=0) twice the strain of rate forces, which allows the threshold to avoid boundary layers, where strain of rate forces remains high.

Indeed, using the equation (23) and the definition of the velocity gradient tensor, we obtain (Holmén, 2012):

$$Q = \frac{1}{2}\,|\bar{\bar{\Omega}}|+|\bar{\bar{S}}|$$

On the figures 3.2 and 3.4, we can clearly see the same small eddies formation above the airfoil for the MEDIUM mesh than the one found in the literature. Although the iso contours displayed are bigger downstream the airfoil in the literature, eddies above the airfoils are similar in shape and vorticity magnitude's distribution for both meshes, on the figures 3.2 and 3.4. In contrast, the COARSE mesh displays cylindrical eddies that stay well organized, far from what we expect of turbulence flow. Compared to the MEDIUM mesh, the FINE mesh's iso contours on figure 3.3, does not show much differences. Small eddies as well as bigger ones are well displayed, if we compare to figure 3.3 from the literature. However, we can notice that the vorticity magnitude is higher on a longer part of the airfoil than with the MEDIUM mesh. Indeed, the area between 3000 rotations per second and 6000 rotations per seconds (in green) grows with mesh refinement. Green area does practically not exist for the COARSE mesh on figure 3.1, and appears figure 3.2 on the MEDIUM mesh. The area with this range of magnitude grows bigger for the FINE mesh.

The Figures 4 present the mean separation bubble for the three meshes. As expected, the COARSE mesh fails in representing the reattachment of the separation bubble and presents a fully stalled airfoil. Indeed, on Figure 4.1, the streamlines do not reattach to the airfoil, and the separation bubble length extends until the trailing edge. In contrast, the Figures 4.2 and 4.3 clearly show a reattachment of the streamlines, around 40%c, as well as the second separation bubble at the rear.

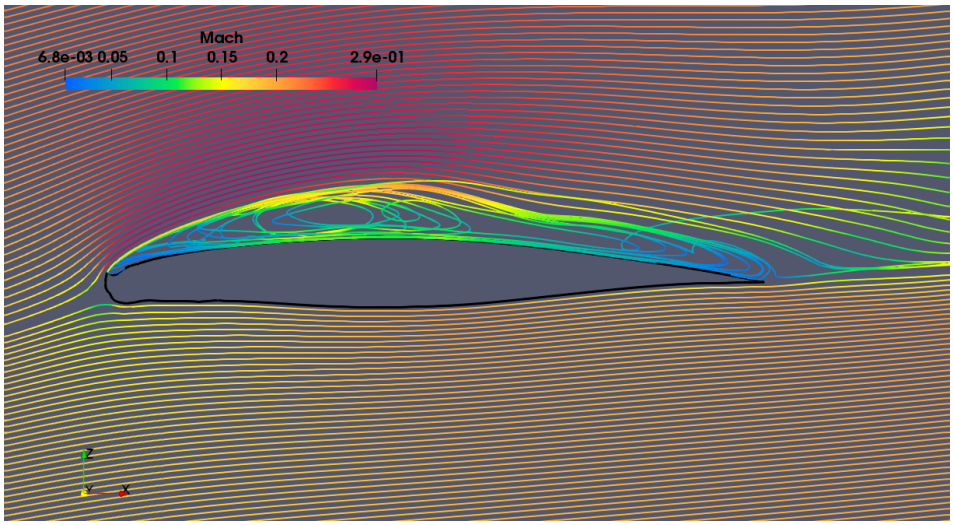

Figure 4.1 : Mean streamlines and mean bubble of separation averaged over 10000 timesteps, COARSE

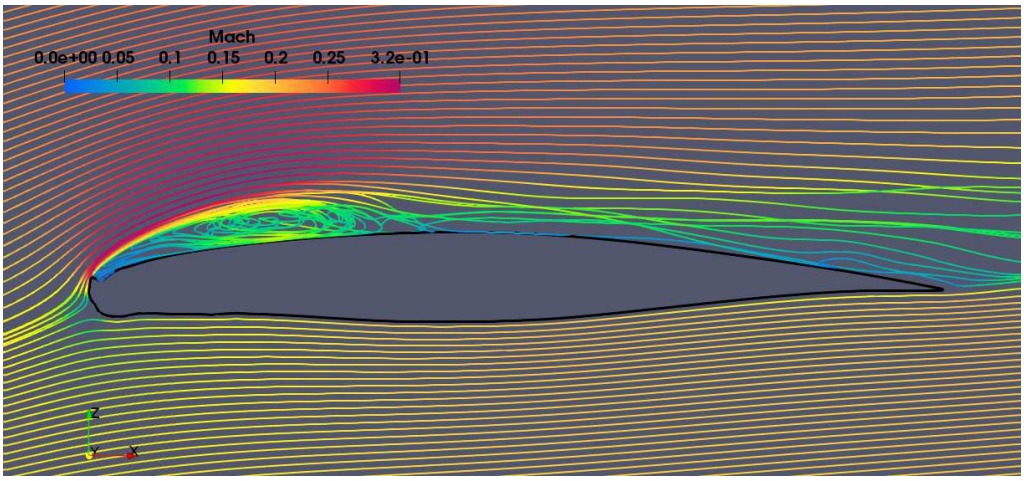

Figure 4.2 : Mean streamlines and mean bubble of separation averaged over 4000 timesteps, THE MEDIUM

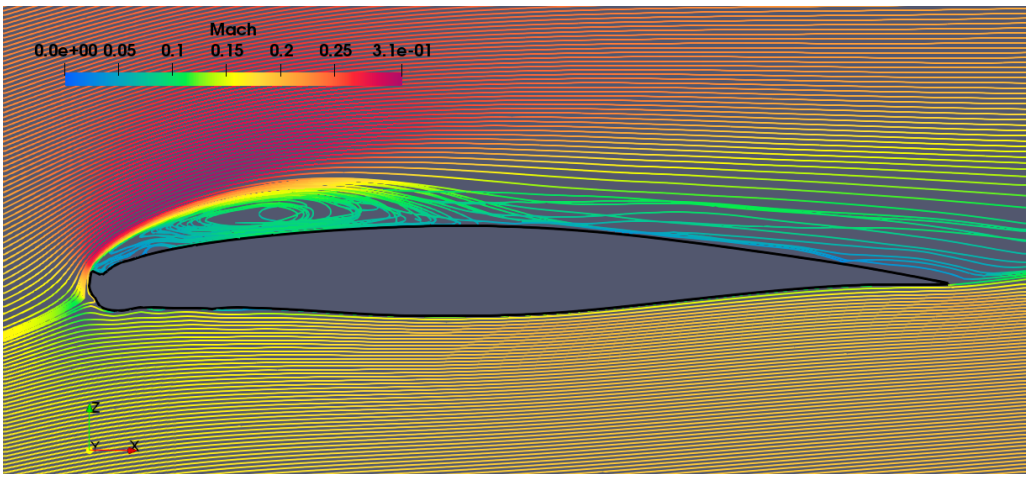

Figure 4.3: Mean streamlines and mean bubble of separation averaged over 28000 timesteps FINE

In order to have a better visualisation of the bubble reattachment localisation depending on the mesh, the graph on figure 5 presents the corresponding mean friction coefficients on x along the airfoil, for the COARSE (blue), MEDIUM (green) and FINE (black) meshes. The region of interest is the x location where Cf changes from negative to positive values and *vice versa*.

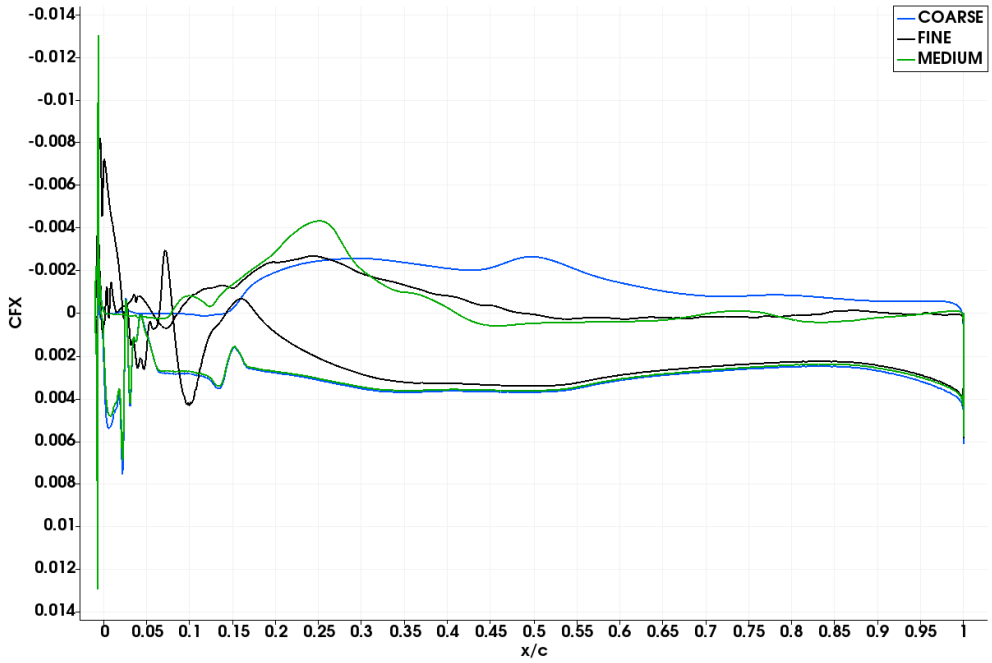

Figure 5 : Mean friction coefficient's comparison of the COARSE, MEDIUM and FINE meshes

As previously seen with the prediction of the CP distribution along the airfoil, on figure 2, the COARSE mesh predicts a fully detached airfoil. Indeed the Cf, in blue, from 15%c until trailing edge, are in negative values. The MEDIUM mesh's Cf remains negative until 40%c, and then again between 70%c and 80%c. This second area is what has been identified on figure 4.2 as the second separation bubble. The FINE mesh's separation extends longer on the chord length, as CF are in the negative values until 48%c. The second separation bubble is also located closer to the rear of the airfoil, between 85%c and 90%c.

Conclusion

We discussed and compared general aspect of vorticities structures of the COARSE, MEDIUM and the FINE meshes, with the iso-contours Q-criterion, mean aerodynamic coefficients have been compared against experimental data and literature. After validation and verification cases, the COARSE mesh has been found to be too coarse to be suitable for DDES. When comparing the mean aerodynamic coefficients results, we found that spanwise grid density has a great influence over their value, when using a spanwise step coarser than $\Delta y/c=0.01$. Though mean CL gives good results with a coarser mesh, mean CP distribution, as well as mean CD, failed to predict experimental data. Good accuracy (below or equal to 1% relative error for mean CL and 5% relative error for mean CD) are obtained using a spanwise step $\Delta y/c=0.01$ or finer. Concomitantly, the mean separation bubble already shows good results for the MEDIUM mesh, with a reattachment at 40%c, whereas the COARSE mesh predicted a fully detached airfoil.

According what has been discussed in the article, the best compromise regarding resources consumption (mesh size) and accuracy of aerodynamics' coefficients had been obtain with the MEDIUM mesh, using a spanwise step of $\Delta y/c=0.01$. This configuration allows us to get below 0.2% of relative error against experimental data for lift coefficient, and 4.1% for drag coefficient, with 60000 iterations and time step of 5E-6s.

More efforts must be put to average on a longer period. Blur about how to set an efficient average range makes harder the comparison of mean values from different studies. In the future, some investigation regarding criterion defining a suitable average range to calculate mean values would be interesting, as literature is not clear about that.

A finer mesh could be interesting to test, with a spanwise step between 0.006 and 0.002, to see whether the tendency is confirmed for the evolution of drag coefficient relative error.

Simulations have been carried out using Compute Canada clusters, MCIA (Mésocentre de Calcul Intensif Aquitain) facilities and the PLaFRIM experimental testbed. PLaFRIM cluster is being developed under the Inria PlaFRIM development action with support from LABRI and IMB and other entities:

Conseil Régional d'Aquitaine (http://aquitaine.fr/),
FeDER
(http://europa.eu/legislation_summaries/employment_and_social_policy/job_creation_measures/l60015_fr.htm)
Université de Bordeaux
(http://www.univ-bordeaux.fr/)
and CNRS
(http://www.cnrs.fr/, see https://plafrim.bordeaux.inria.fr/).

We thank Compute Canada and Inria PlaFRIM for making this study possible.

Bibliography

Alam, M. F., Thompson, D. S., & Walters, D. K. (2015). Hybrid Reynolds-Averaged Navier–Stokes/Large-Eddy Simulation Models for Flow Around an Iced Wing. *Journal of Aircraft, 52*(1), 244-256. doi:10.2514/1.C032678

Bonnet, J. P. (1996). *Eddy Structure Identification* (J. P. Bonnet Ed.). International Center for Mechanical Sciences: Springer-Verlag Wienn.

Butler, C., Qin, C., & Loth, E. (2016). *Improved Delayed Detached-Eddy Simulation on a Swept Hybrid Model in IRT*. Paper presented at the 8th AIAA Atmospheric and Space Environments Conference.

Chong, M. S., Perry, A. E., & Cantwell, B. J. (1990). A general classification of three dimensional flow field. In *Physics of Fluids A: Fluid Dynamics* (Vol. 2): American Institute of Physics.

Deck, S. (2011). Recent improvements in the Zonal Detached Eddy Simulation (ZDES) formulation. *Theoretical and Computational Fluid Dynamics, 26*(6), 523-550. doi:10.1007/s00162-011-0240-z

Forsythe, J. R., Squires, K. D., Wurtzler, K. E., & Spalart, P. R. (2004). Detached-Eddy Simulation of the F-15E at High Alpha. *Journal of Aircraft, 41*(2), 193-200. doi:10.2514/1.2111

GARTEUR. (2003). *Prediction of Performance Degradation due to Icing for 2D Configurations* (AG-32). Retrieved from

Holmén, V. (2012). *Methods for Vortex Identification.*

Hu, S., Zhang, C., Liu, H., Wang, F., & Li, Y. (2018). *IDDES simulation of flow separation on an 3-D NACA23012 airfoil with spanwise ridge ice*. Paper presented at the 2018 Atmospheric and Space Environments Conference.

Hunt, J. C. R., Wray, A. A., & Moin, P. (1988, 11 1988). *Eddies, streams, and convergence zones in turbulent flows*. [Fluid Mechanics and Heat Transfer]. (2). Studying Turbulence Using Numerical Simulation Databases, 2. Proceedings of the 1988 Summer Program.

Liang, Z.-c., & Xue, L.-p. (2014). Detached-eddy simulation of wing-tip vortex in the near field of NACA 0015 airfoil. *Journal of Hydrodynamics, 26*(2), 199-206. doi:10.1016/s1001-6058(14)60022-6

Lorenzo, A., Valero, E., & de-Pablo, V. (2011). *DES/DDES post-stall study with iced airfoil*. Paper presented at the American Institute of Aeronautics and Astronautics, Orlando, Florida.

Mockett, C. (2009). *A comprehensive study of detached-eddy simulation.* (Doctor Engineer Dissertation), Technischen Universität Berlin,

Molina, E., & Silva, R. G. A. (2017). *An Overview Of DDES In SU2*. Paper presented at the 2nd Annual SU2 Developers Meeting,.

Molina, E., Spode, C., Annes da Silva, R. G., Manosalvas-Kjono, D. E., Nimmagadda, S., Economon, T. D., . . . Righi, M. (2017). *Hybrid rans/les calculations in su2.* Paper presented at the 23rd AIAA Computational Fluid Dynamics Conference.

Oztekin, E. S., & Riley, J. T. (2018). *Ice accretion on a NACA 23012 airfoil*. Paper presented at the 2018 Atmospheric and Space Environments Conference.

Pan, J., & Loth, E. (2004). *DETACHED EDDY SIMULATIONS FOR AIRFOIL WITH ICE SHAPES*. Paper presented at the 42nd AIAA Aerospace Sciences Meeting and Exhibit, Reno, Nevada.

Pan, J., & Loth, E. (2005). Detached Eddy Simulations for Iced Airfoils. *Journal of Aircraft, 42*(6), 1452-1461. doi:10.2514/1.11860

Shur, M. L., Spalart, P. R., Strelets, M. K., & Travin, A. K. (2015). An Enhanced Version of DES with Rapid Transition from RANS to LES in Separated Flows. *Flow, Turbulence and Combustion, 95*(4), 709-737. doi:10.1007/s10494-015-9618-0

Spalart, P. (2000). Strategies for turbulence modelling and simulations. *International Journal of Heat and Fluid Flow, 21*, 252-263. doi:10.1016/S0142-727X(00)00007-2

Spalart, P., & Allmaras, S. (1992). *A one-equation turbulence model for aerodynamic flows* (AIAA Paper 1992-439). Retrieved from https://doi.org/10.2514/6.1992-439

Spalart, P., & Allmaras, S. (1994). A One-Equation Turbulence Model for Aerodynamic Flows. *Recherche Aérospatiale, 1*, 5-21.

Spalart, P., Jou, W., Strelets, M., & Allmaras, S. (1997). *Comments on the feasibility of LES for wings, and on a hybrid RANS/LES approach*. Paper presented at the Advances in DNS/LES First AFOSR International Conference on DNS/LES, Lousinia.

Spalart, P., W.Jou, Strelets, M., & Allmaras, S. (1997). Comments on the feasibility of LES for wings, and on a hybrid RANS/LES approach. *Advances in DNS/LES, 1*.

Spalart, P. R., Deck, S., Shur, M. L., Squires, K. D., Strelets, M. K., & Travin, A. (2006). A New Version of Detached-eddy Simulation, Resistant to Ambiguous Grid Densities. *Theoretical and Computational Fluid Dynamics, 20*(3), 181-195. doi:10.1007/s00162-006-0015-0

Tagawa, G. B. S., Morency, F., & Beaugendre, H. (2018). *CFD study of airfoil lift reduction caused by ice roughness*. Paper presented at the AIAA.

White, F. M. (2006). *Viscous fluid flow* (3rd ed.). New York, NY: McGraw-Hill Higher Education.

Xiao, M., Zhang, Y., & Chen, H. (2017). *Numerical Study of an Iced Airfoil Using Window-Embedded RANS/LES Hybrid Method*. Paper presented at the 9th AIAA Atmospheric and Space Environments Conference.

Zhang, Y., Habashi, W. G., & Khurram, R. A. (2016). Zonal Detached-Eddy Simulation of Turbulent Unsteady Flow over Iced Airfoils. *Journal of Aircraft, 53*(1), 168-181. doi:10.2514/1.C033253